JACS
JOURNAL OF THE AMERICAN CHEMICAL SOCIETY

Article

pubs.acs.org/JACS

One-Step Synthesis of Cross-Linked Ionic Polymer Thin Films in Vapor Phase and Its Application to an Oil/Water Separation Membrane

Munkyu Joo,[†] Jihye Shin,[†] Jiyeon Kim, Jae Bem You, Youngmin Yoo, Moo Jin Kwak, Myung Seok Oh, and Sung Gap Im*

Department of Chemical and Biomolecular Engineering, Korea Advanced Institute of Science and Technology (KAIST), Daejeon 34141, Korea

Supporting Information

ABSTRACT: In spite of the huge research interest, ionic polymers could not have been synthesized in the vapor phase because the monomers of ionic polymers contain nonvolatile ionic salts, preventing the monomers from vaporization. Here, we suggest a new, one-step synthetic pathway to form a series of cross-linked ionic polymers (CIPs) in the vapor phase *via* initiated chemical vapor deposition (iCVD). 2-(Dimethylamino)ethyl methacrylate (DMAEMA) and 4-vinylbenzyl chloride (VBC) monomers are introduced into the iCVD reactor in the vapor phase to form a copolymer film. Simultaneously in the course of the deposition process, the tertiary amine in DMAEMA and benzylic chloride in VBC undergo a Menshutkin nucleophilic substitution reaction to form an ionic ammonium−chloride complex, forming a highly cross-linked ionic copolymer film of p(DMAEMA-*co*-VBC). To the best of our knowledge, this is the first report on the synthesis of CIP films in the vapor phase. The newly developed CIP thin film is further applied to the surface modification of the membrane for oil/water separation. With the hydrophilic and underwater oleophobic membrane whose surface is modified with the CIP film, excellent separation efficiency (>99%) and unprecedentedly high permeation flux (average 2.32 × 10^5 L m^{-2} h^{-1}) are achieved.

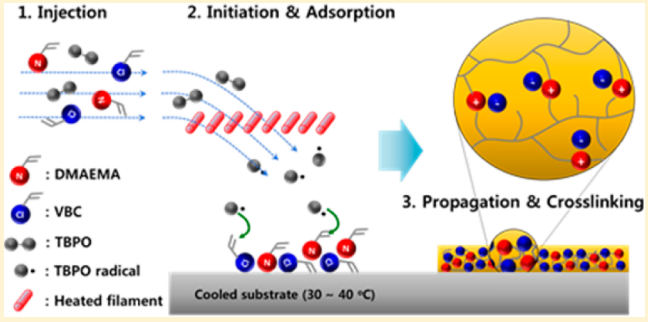

INTRODUCTION

Ionic polymers have received great attention in the field of polymeric material science due to their own unique advantageous properties,[1−3] including ion conductivities,[4,5] ion exchange properties,[3,6] nonflammability,[7] and corrosion inhibition properties,[8] which all commonly originate from the ionic salts in the polymer. Recently, ionic polymers have been applied to various fields such as electronic devices,[9,10] electrochemical sensors,[11] electrolytes for batteries,[12] membranes for fuel cells,[13,14] polymer actuators,[15] and antimicrobial coatings.[16,17]

To date, the ionic polymers have been synthesized in the solution phase, which involves multistep synthesis followed by complex purification procedures. Moreover, most of ionic polymers are highly soluble in polar organic solvents, including water, due to the polar ionic functionalities in the polymer chain. Hence, cross-linking of ionic polymers was attempted in order to improve the chemical and mechanical stability of the ionic polymers by adding cross-linker molecules.[18,19] However, the cross-linking significantly limits the polymer chain mobility and thus the processability of the polymer.[20] Vapor-phase synthesis of cross-linked ionic polymers (CIPs) can resolve most of the problems noted above. Previous reports showed that the polymers synthesized in situ in a vapor phase reactor can form a pinhole-free, uniform thin film that conformally covers various nonflat surfaces with micro- or nanoscale structures.[20] However, the synthesis of ionic polymers in the vapor phase have not yet been possible because the monomers with ionic functionalities commonly show negligible vapor pressure due to the nonvolatile ionic components.[21]

Here, in order to overcome this problem, a new synthetic route to form CIPs in the vapor phase is suggested (Figure 1a). We adopted a vapor-phase polymerization method, termed initiated chemical vapor deposition (iCVD). The iCVD process utilizes a radical polymerization reaction to fabricate polymeric thin films from vaporized monomers and an initiator.[22] The injected monomers are adsorbed on the surface of substrate, and the free radicals formed by thermal decomposition of the initiator are delivered to the adsorbed monomers. Finally, a polymer thin film grows on the substrate surface, resulting in a dewetting-free, highly conformal film maintaining the initial surface morphology of the substrates. For the synthesis of CIPs in the vapor phase, however, it is necessary to design a new

Received: November 1, 2016
Published: January 24, 2017

DOI: 10.1021/jacs.6b11349
J. Am. Chem. Soc. 2017, 139, 2329−2337

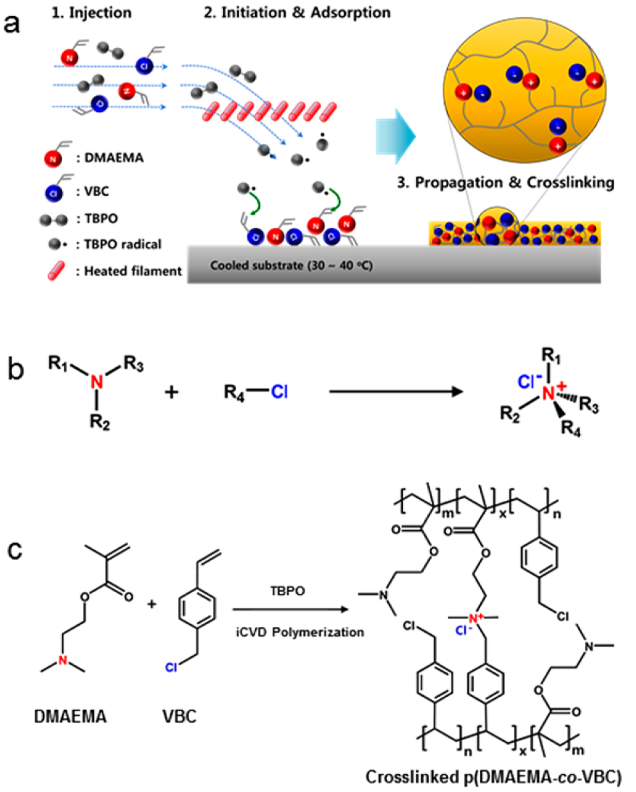

Figure 1. (a) Synthetic concept of cross-linked ionic polymers using the iCVD polymerization process. (b) Scheme of the Menshutkin reaction. (c) Synthetic scheme and chemical structure of cross-linked ionic p(DMAEMA-*co*-VBC) copolymer. The *m* and *n* represent the unreacted contents of DMAEMA and VBC, respectively. The *x* is the ionic cross-linked part generated through the Menshutkin reaction. These *m*, *n*, and *x* values are changed by feed ratios of each monomer into the iCVD chamber.

synthetic method to incorporate ionic components in the polymer chain because the monomers with ionic components are hardly vaporizable.

In this study, for the formation of ionic functionalities in the vapor phase, we chose two kinds of monomers without ionic species, thus both reactants are readily vaporizable. By vaporizing the two monomers into the iCVD chamber, we attempted to trigger an ionic cross-linking reaction simultaneously with an iCVD polymerization reaction in a one-step manner, which was designed so that the process does not require any additional cross-linker. For this purpose, we utilized an in situ ionic cross-linking reaction between a tertiary amine-containing monomer as a nucleophile and an alkyl halide-containing monomer as an electrophile to induce the quaternarization of the tertiary amine. To optimize the ionic cross-linking density, the reactivity of each monomer was investigated. As a result, we can synthesize highly uniform CIP thin films in situ with controlled thickness and large-area uniformity. The CIP showed hydrophilic and water-absorbing properties. The CIP synthesized in this work also showed an excellent chemical stability against most of the organic solvents. The CIP films maintained their hydrophilicity even with the increased cross-linking density, which is a unique characteristics of the iCVD CIP films; the increase of cross-linking density renders the CIP still hydrophilic.

To utilize this unique advantageous characteristic of the iCVD CIP film, the copolymer thin film was applied to the surface modification of the membrane for oil/water separation by incorporating underwater oleophobicity to the membrane.[23] For this purpose, the surface of the membrane should retain sufficient hygroscopic property to trap water molecules.[24−26] The water-entrapped surface of the membrane empowers the repulsion of oil from the surface under water. Therefore, water can pass through the hydrated membrane, while oil is rejected from the membrane surface due to the underwater oleophobic property of the membrane. The water-absorbing iCVD CIP film enables the efficient oil/water separation. In addition, the chemical inertness of the iCVD CIP film against various chemical solvents provides the membrane with long-term stability to prevent solubilization or delamination of the CIP films from the membrane.[23]

In this work, the iCVD CIP film was conformally coated on a metal mesh membrane. The surface-modified membrane showed superior underwater oleophobicity. Furthermore, the pore size of the mesh remained unchanged even after immersion in the water, confirming the excellent chemical stability of the iCVD CIP film on the membrane. As a result, the membrane showed unprecedentedly high separation flux with high separation efficiency in an oil/water mixture.

EXPERIMENTAL SECTION

Materials. 4-Vinylbenzyl chloride (VBC, 90%) and *tert*-butyl peroxide (TBPO, 98%) were purchased from Sigma-Aldrich. 2-(Dimethylamino)ethyl methacrylate (DMAEMA, 95%) was purchased from TCI Chemicals and used without further purifications. To analyze the properties of the polymeric thin films, the polymeric films were deposited onto glass slides (Marienfeld, Inc.) or Si wafers (Siltron, Inc.). Hexane (95%), hexadecane (99%), and toluene (99.5%) were purchased from Daejeong, Aldrich, and OCI, respectively.

Synthesis of Poly[2-(dimethylamino)ethyl methacrylate-*co*-4-vinylbenzyl chloride)], Copolymers I, II, and III via iCVD. For synthesis of poly[2-(dimethylamino)ethyl methacrylate-*co*-4-vinylbenzyl chloride] [p(DMAEMA-*co*-VBC)], the target substrate which is placed to deposit polymeric films was first located into the iCVD chamber (Daeki Hi-Tech, Inc.), and the temperature of the substrate was kept at 38 °C for the uniform adsorption of monomers during the iCVD process. The substrate temperature is highly related to the morphology and conformality of the film.[27] Then, DMAEMA and VBC as monomers and TBPO as an initiator were introduced into the iCVD. To deliver each reactant into the iCVD chamber, the DMAEMA, VBC, and TBPO were evaporated at 35, 50, and 25 °C, respectively. To make copolymers with different monomer ratio, the feed ratio of each monomer (DMAEMA/VBC) was adjusted by a needle valve. For copolymer I, the feed ratio of DMAEMA, VBC monomer, and TBPO initiator was maintained at 0.8, 0.4, and 0.3 sccm, respectively. In copolymer II, the ratio of DMAEMA and VBC monomer was kept at 0.6 and 0.6 sccm. In copolymer III, the ratio was kept at 0.4 and 0.8 sccm, respectively. In this experiment, the flow rate of the initiator was fixed at 0.3 sccm.[28] At the same time, the chamber pressure was kept at 150 mTorr using a throttle valve, and then the temperature of the filament was heated to 180 °C to make TBPO radicals for the free radical polymerization reactions. The film thickness was monitored in situ by a He−Ne laser (JDS Uniphase) interferometer.

Characterizations. To examine the properties of synthetic films, several analyses were conducted. Fourier transform infrared spectroscopy (FT-IR) was measured using the ALPHA FT-IR (Bruker Optics) instrument in absorbance mode, with 64 scans collected for each spectrum to confirm whether polymerization occurred or not after the iCVD polymerization process. To clarify evidence that the cross-linked ionic polymer was synthesized in the iCVD chamber, the X-ray photoelectron spectroscopy (XPS) (Sigma Probe, Thermo VG Scientific Inc.) measurements were performed. The cross-linking

DOI: 10.1021/jacs.6b11349
J. Am. Chem. Soc. 2017, 139, 2329−2337

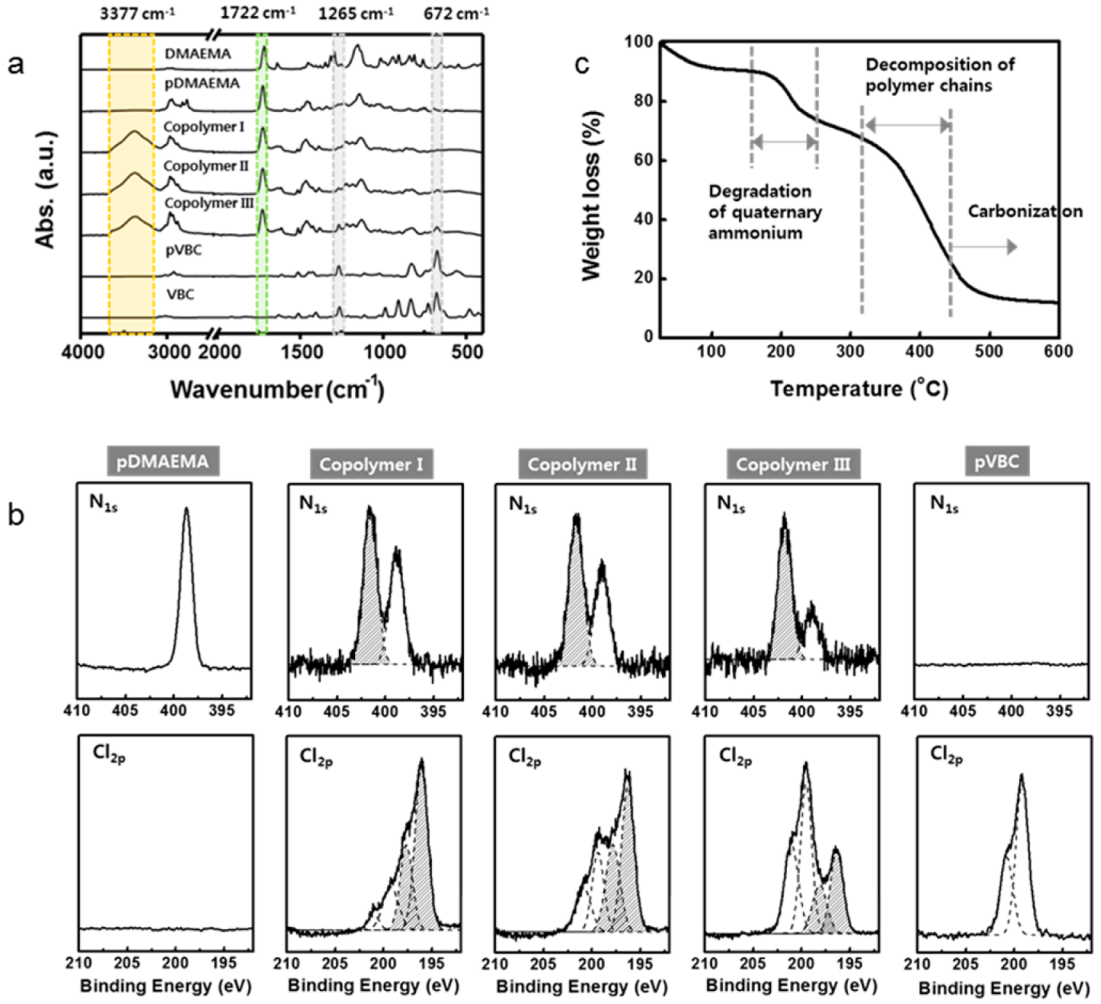

Figure 2. (a) FT-IR spectra of the DMAEMA monomer, pDMAEMA, p(DMAEMA-*co*-VBC) copolymers I, II, and III, pVBC, and VBC monomer (from top to bottom). (b) XPS high-resolution scan of N_{1s} (top) and Cl_{2p} (bottom) of pDMAEMA, p(DMAEMA-*co*-VBC) copolymers I, II, and III, and pVBC. The gray regions represent the peaks related to the N^+ peak in N_{1s} spectra and Cl^- peaks in Cl_{2p} spectra. (c) Thermogravimetric analysis curve of p(DMAEMA-*co*-VBC) copolymer I.

degree can be expressed by quaternary ammonium (N_{1s}^+) contents, which can be calculated by dividing the atomic percent of N_{1s}^+ by the sum of the atomic percent of the elements that participate in the cross-linking reaction and the unreacted elements [N_{1s}^+, Cl_{2p} + (N_{1s}^+ or Cl_{2p}^-)]. Generally, in XPS spectra, the N_{1s}^+ ion peak is observed at 402 eV and the Cl_{2p}^- ion peaks are observed at 196 and 197 eV binding energy regions.[29−31] Thermogravimetric analysis (TGA) was measured in the range from 25 to 600 °C (heating rate was maintained at 20 °C/min) to obtain the thermal property of the ionic polymer using a Mettler-Toledo TGA instrument. To ensure the p(DMAEMA-*co*-VBC) deposition on the substrates after the iCVD process, the water contact angles (WCAs) and underwater−oil contact angles (OCAs) were measured after achieving a static equilibrium state using a contact angle analyzer (Phoenix 150, SEO, Inc.). The volume of an individual water droplet was 10 μL. Each WCA or underwater OCA value was obtained from the average data of more than five different positions in the same sample. We used 1,2-dichloroethane (10 μL) (anhydrous, 99.8%, Aldrich, USA) stained with oil red O as a detecting oil for measuring underwater OCAs. Although most oils usually float above water, due to the high density of 1,2-dichloroethane, the OCA was directly measured without special auxiliary equipment. To measure the underwater OCA of the p(DMAEMA-*co*-VBC)-coated membrane, the membrane was submerged underwater in a completely transparent container. Images of the surface of the p(DMAEMA-*co*-VBC)-coated mesh were observed using field-emission scanning electron microscopy (FE-SEM, FEI) with an operating voltage of 10 kV. To analyze the surface roughness of the coating, atomic force microscope (AFM) images were taken using a scanning probe microscope (SPM) (XE-100, Park system) at a scan size of 2 × 2 μm squares.

Oil/Water Separation. Before the separation test, the p-(DMAEMA-*co*-VBC)-coated mesh was fully soaked in deionized water over 20 min. The water-absorbed membrane was put between two glass cylinders (diameter, 37.30 mm). The oils (hexane, hexadecane, and toluene) were colored with oil red O for better visualization. Each 250 mL of oil/water mixture (20% v/v) was poured into the apparatus for separation performance analysis. The separation efficiency (E_s) of each oil mixture was calculated using the equation below:

$$E_s\ (\%) = \frac{M_{\text{filtrate}}}{M_{\text{mixture}}} \times 100 \tag{1}$$

where M_{filtrate} and M_{mixture} are determined by the mass of water in the filtrate and original oil/water mixture, respectively.

The water flux (F) was calculated by measuring the time for 1 L of water to pass through 50 mL of hexane on the membrane. The water flux was calculated from the following equation:

$$F = \frac{V}{S \cdot t} \tag{2}$$

DOI: 10.1021/jacs.6b11349
J. Am. Chem. Soc. 2017, 139, 2329−2337

Table 1. Summarized Data of Calculated Ionic Cross-Linking Degrees Derived from High-Resolution XPS Spectra

	feed ratio[a]	copolymer ratio[b]	moiety (unit) contents (%)[c]			
polymer	DMAEMA/VBC	DMAEMA/VBC	N_{1s} (m)	Cl_{2p} (n)	N_{1s}^{+}/Cl_{2p}^{-} (x)	cross-linking degrees (%)[d]
copolymer I	2:1	1.3:1	36	14	50/51	50.5(±0.5)
copolymer II	1:1	1:1	29	25	46/47	46.5(±0.5)
copolymer III	1:2	1:2.2	11	58	31/33	32.5(±1.0)

[a]The ratio of the amount of each monomer to be introduced into the iCVD chamber. [b]The actual proportion of each monomer included in the copolymers. [c]The data from the deconvolution of high-resolution XPS data, N, Cl: non-cross-linked (unreacted) *tert*-amine and VBC monomer contents, N^+, Cl^-: relate to cross-linked component. [d]Average value of N^+ and Cl^- contents.

where V is the volume of water that passes through the membrane, S is the cross-sectional area of the membrane that water contacts, and t is the time for the passing of 1 L of water through the membrane. The measurement was conducted with five different membranes.

The breakthrough pressure of the membrane was estimated according to the following equation:

$$P = \rho g h_{max} \quad (3)$$

where ρ is the density of hexane, g is the acceleration of gravity, and h_{max} is the maximum height of the hexane cylinder that the membrane can endure.

The purity of the filtrate was analyzed by Karl Fischer method (ISO 760:2007).

RESULTS AND DISCUSSION

For the formation of ionic cross-linking sites, we utilized the Menshutkin reaction between tertiary amine-containing and alkyl halide-containing monomers to generate the quaternary ammonium chloride, which serves as the cross-linking sites (Figure 1b). Therefore, the Menshutkin reaction can render the polymer cross-linked ionically to complete the synthesis of CIP. However, it is reported that the Menshutkin reaction is not favorable in the vapor phase compared to that in the solution phase because the use of polar solvents is known to be essential for enhancing the reaction rate.[32−34] Therefore, in the solvent-free vapor phase, the monomers with high reactivity must be employed for the synthesis of CIPs *via* the Menshutkin reaction. In this regard, we chose 2-(dimethylamino)ethyl methacrylate (DMAEMA) as a nucleophile and 4-vinylbenzyl chloride (VBC) as an electrophile (Figure 1c). The DMAEMA has a strong nucleophilic characteristic due to its tertiary amine moiety, whereas the VBC is a good electrophile due to the resonance-induced stability effect of benzylic carbon.[35−37] Since each monomer does not contain any ionic species, both reactants are readily vaporizable.

Before the synthesis of CIP via the iCVD process, iCVD polymerization of poly(4-vinylbenzyl chloride) (pVBC) from the VBC monomer was checked via FT-IR spectroscopy (Figure S1 in the Supporting Information). The stretching (1630 cm^{-1}) and bending peaks (908 cm^{-1}) of the C═C disappear after the polymerization, indicating successful radical polymerization in the iCVD chamber. Also, we clearly observed the stretching and bending peaks of C−Cl at 1265 and 672 cm^{-1}, respectively. This result demonstrates that the highly reactive benzylic chloride in the VBC monomer[36,37] was maintained in the pVBC film, suggesting that the iCVD process does not damage the pendent functionalities in the monomer, which is fully consistent with previous observations.[20,22] Analogously, the poly(2-(dimethylamino)ethyl methacrylate) (pDMAEMA) homopolymer was also synthesized via the iCVD process, and the retention of the tertiary amine moiety in the iCVD polymer film was also confirmed by checking the FT-IR spectra of the DMAEMA monomer and the corresponding polymer film (Figure 2a).[38]

For the synthesis of the CIP film, we introduced DMAEMA along with VBC into the iCVD chamber (Figure 1), where the copolymerization of the vaporized monomers via free radical polymerization reaction and the nucleophilic substitution reaction with tertiary amine in DMAEMA and alkyl chloride in VBC occurred simultaneously to form the CIP film. In order to optimize their cross-linking degree of the CIP, the feed ratio of each monomer was adjusted; the ratio of DMAEMA to VBC was set to 2:1 (copolymer I), 1:1 (copolymer II), and 1:2 (copolymer III).

To confirm the deposition of ionically cross-linked copolymer films, the FT-IR and XPS analyses were conducted on the deposited polymer films. Figure 2a shows the FT-IR spectra of pDMAEMA, pVBC, and the ionic copolymer, p(DMAEMA-*co*-VBC), with various feed ratios. In the FT-IR spectra of all copolymer films, the carbonyl (C═O) peak from the DMAEMA at 1722 cm^{-1} and the C−Cl peak from the VBC at 672 cm^{-1} were commonly detected, indicating that the copolymerization occurred successfully in the vapor phase.

The intensity of each peak was changed with respect to the input flow rate of each monomer. Moreover, the spectra for all of the synthesized copolymers displayed a broad band at 3377 cm^{-1} that is related to hydroxyl functionality, whose intensity was also changed in accordance with the feed ratio. This peak is associated with the binding of water molecules on the quaternary ammonium groups to form the cross-linked moiety.[39]

The surface compositions of copolymers I, II, and III were calculated from the XPS survey scan (Figure S2 in the Supporting Information), considering that the copolymers contain each characteristic element of N in DMAEMA and Cl in the VBC repeating unit in the copolymers. When the contents of DMAEMA/VBC in copolymers I, II, and III were analyzed, the estimated surface composition ratios between the two monomers were DMAEMA/VBC = 1.3:1, 1:1, and 1:2.2, respectively. The difference between the input feed ratio and the resultant composition ratio of the copolymer is due to the vapor-pressure (VP) difference of each monomer (VP_{DMAEMA} ∼ 600 mTorr, VP_{VBC} ∼ 100 mTorr at 25 °C), which affects the concentration of the amount of the adsorbed monomers on target substrates, which in turn affects the polymerization rate of each component in the iCVD process.[40]

In the XPS spectra of homopolymers of pDMAEMA and pVBC, only N and Cl peaks were observed but no N^+ and Cl^- contents were detected (Figure 2b). On the other hand, newly emerged N^+ and Cl^- peaks were all commonly observed in the high-resolution XPS spectra in the p(DMAEMA-*co*-VBC) copolymers, which also confirmed that an ionic complex ($-NR_3^+Cl^-$) was generated by the cross-linking reaction during the iCVD process (Figure 2b). The feed rate variation of each

DOI: 10.1021/jacs.6b11349
J. Am. Chem. Soc. 2017, 139, 2329−2337

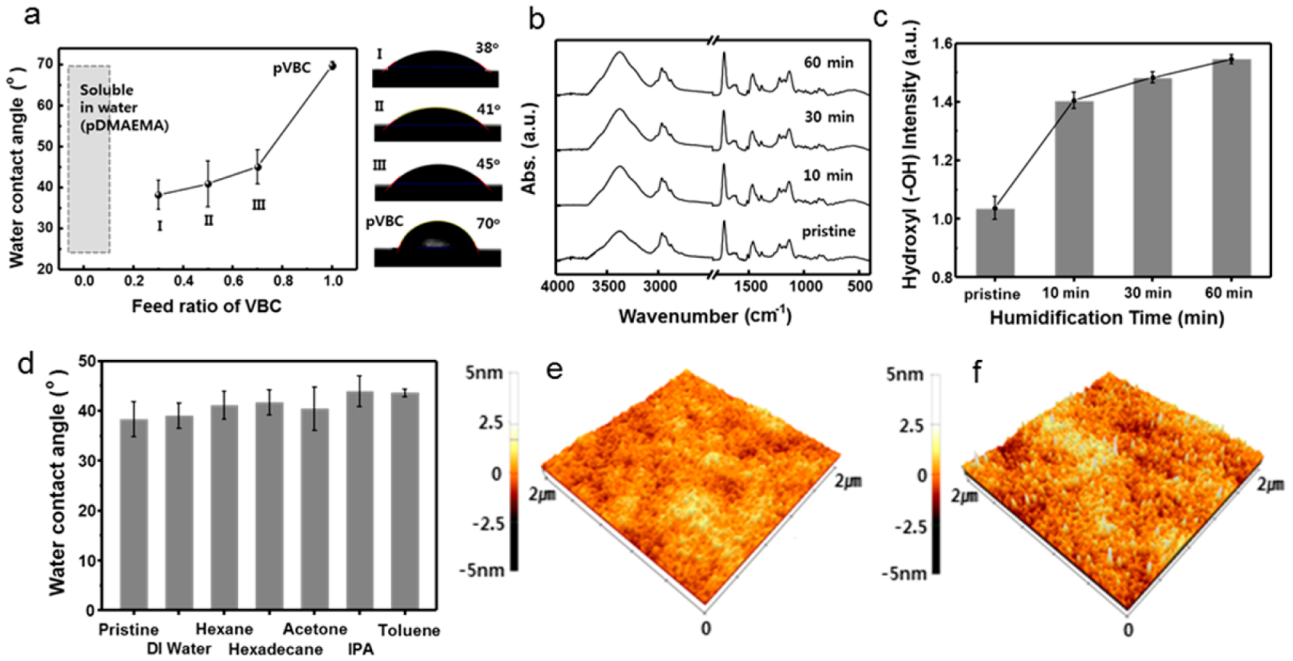

Figure 3. (a) Water contact angle values of pDMAEMA, p(DMAEMA-*co*-VBC) copolymers I, II, and III and pVBC films on Si wafers according to flow ratio of each monomer. (b) FT-IR spectra of copolymer I films at 38 °C, 90% RH for 0 (pristine), 10, 30, and 60 min. (c) Relative intensity values of hydroxyl (−OH) peaks vs humidification time. (d) WCA values of copolymer I films on Si wafer after being soaked in DI water, hexane, hexadecane, acetone, IPA, and toluene for 48 h. The AFM images of p(DMAEMA-*co*-VBC) and copolymer I film on a Si wafer before (e) and after (f) being soaked in acetone for 48 h.

monomer resulted in the change of quaternary ammonium (N^+) contents in the p(DMAEMA-*co*-VBC) polymers, and the calculated N^+ percentage of copolymers I, II, and III were 50, 46, and 31%, respectively. The results of XPS analysis are summarized in Table 1. It is worthwhile to mention that both the Menshutkin reaction and free radical polymerization reaction are all addition reactions without leaving any byproduct, which is extremely advantageous in that the polymer film does not require any post-purification procedure. Since the synthesis method does not involve any solvents or additives, we could fabricate ionic polymer films with extreme purity.[41]

As mentioned above, the Menshutkin reaction is not favorable in the vapor phase, due to the dominance of Coulombic interactions between two reactants. Therefore, without a solvation effect, additional energy input is generally required in order for the reaction to overcome the activation energy barrier.[33] To assess the reactivity of the Menshutkin reaction in the vapor phase, 2-chloroethyl acrylate (CEA) replaced VBC as the electrophile to react with DMAEMA in the iCVD chamber (Figure S3 in the Supporting Information). Because CEA also contains 1° alkyl halide as does VBC, the reactivity with the nucleophile is expected to be similar to that with VBC in the solution phase.[36] However, to our surprise, the ionic cross-linking reaction between CEA and DMAEMA did not occur in p(CEA-*co*-DMAEMA) during the iCVD process in the vapor phase; no N^+ peak relating to the ionic cross-linking reaction was detected in the XPS spectra (Figure S4 in the Supporting Information). Post-annealing treatment was applied to the deposited p(CEA-*co*-DMAEMA) film at 150 °C for 1 h. Only with the post-treatment could we detect the quaternary ammonium chloride ($-NR_3^+Cl^-$) functionalities in the XPS spectra (Figure S5 in the Supporting Information), which strongly infers that CEA requires higher energy to undergo the Menshutkin reaction with DMAEMA than VBC does. The observation shows that VBC is a better electrophile than CEA because the resonance-induced stability effect of benzylic carbon in VBC plays a role in decreasing activation energy of the Menshutkin reaction in a solvent-free environment. This tendency is consistent with previous simulation studies about Menshutkin reactivity in the gas phase.[32−34,42] However, this result does not imply that this reaction is limited to VBC only. Any monomer substance having a sufficient capability of stabilization of a carbocation by a resonance effect is applicable to the Menshutkin reaction.[37] For example, allylic carbons, tertiary (3°) carbons, and carbons of carbonyl groups can react with nucleophiles in the vapor phase.

The thermogravimetric analysis also supports the fact that the Menshutkin reaction-based ionic cross-linking occurred simultaneously during the iCVD polymerization. In TGA curve of copolymer I [p(DMAEMA-*co*-VBC)] (Figure 2c), three major mass loss steps were observed; the first step is related to the degradation of quaternary ammonium functionalities (160 to 250 °C); the second step represents the decomposition of polymer chain (310 to 450 °C), and the last one corresponds to the carbonization step (above 450 °C). These results are consistent with previous reports on ionic cross-linked polymers synthesized in the liquid phase.[43,44]

Water contact angle was also measured to check the hydrophilicity of the copolymer films (Figure 3a). While pDMAEMA is extremely hydrophilic, considering that the film is soluble in water, the WCA of pVBC was 69.8 ± 1.0°, indicating that pVBC was relatively hydrophobic. Interestingly, the average WCA data of all the copolymers were observed in the narrow range of 38−45°, which are far deviated from linear combination of the copolymer composition; increasing the composition of more hydrophobic VBC did not result in the increase in the hydrophobicity. The copolymer I showed the lowest WCA value of about 38.3 ± 3.5°. This observation

DOI: 10.1021/jacs.6b11349
J. Am. Chem. Soc. 2017, 139, 2329−2337

originates from the polar ionic cross-linking site ($-NR_3^+Cl^-$), which makes the surface more hydrophilic. Therefore, the polymer with the highest cross-linking density showed the most hydrophilicity. Also, the increase in the VBC moiety in the copolymer (copolymer III) still maintained a considerable amount of hydrophilicity. This interesting feature of CIP film leads to the formation of highly cross-linked but still hydrophilic polymer film.

Besides the enhanced hydrophilicity, the CIP film was also highly water-absorbing. The hygroscopic property of the CIP film was further investigated by monitoring the change of hydroxyl peak intensity in FT-IR spectra with respect to the exposure time in a controlled humid condition (38 °C, 90% humidity). As expected, the exposure time increase clearly induced the increase in the peak intensity at 3377 cm^{-1} (Figure 3b,c). The initial 10 min exposure of moisture leads to a sharp increase in the peak intensity. Afterward, only a slight increase was observed up to 60 min exposure, indicating that the water absorption in the copolymer was saturated.

The cross-linking of ionic polymer substantially improves the chemical stability of the polymer film against various harsh solvents. To monitor the solvent resistance of p(DMAEMA-*co*-VBC) film, copolymer I-coated Si wafers were placed in various solvents, including deionized (DI) water, isopropyl alcohol (IPA), acetone, hexane, hexadecane, and toluene for 48 h. The WCA measurements showed that 48 h of solvent treatment caused only negligible changes compared to untreated samples (Figure 3d). The surface of copolymer I-coated Si wafers treated with acetone for 48 h was monitored by AFM and compared to the surface of the untreated sample (Figure 3e,f). The root-mean-squared (rms) roughness of pristine film was only 0.341 nm, without any apparent phase segregation, which confirms a uniform surface property of the copolymer films (Figure 3e). The AFM image clearly demonstrates that the p(DMAEMA-*co*-VBC) film was synthesized homogeneously without forming any apparent phase segregation, which is a unique advantageous characteristic of vapor-phase-synthesized polymer films.[40] The rms roughness of 48-h-treated samples with acetone was also just 0.469 nm, showing the excellent solvent resistance of the CIP films (Figure 3f). Further, the long-term stability of the CIP film was also monitored for 120 h in acetone and hexane. The WCA data and FT-IR spectra of p(DMAEMA-*co*-VBC) film after a 120 h solvent test showed negligible change compared to the pristine film (Figure S6 in the Supporting Information). The observation follows that ammonium chloride-based ionic cross-linking is sufficiently stable to retain superior chemical resistivity against most solvents, which is highly advantageous for various applications to modify surfaces.

Unlike the CIP films synthesized in this study, the hydrophilicity of most cross-linked polymer films decreases with the increase of cross-linking density due to the hydrophobic cross-linking sites from hydrophilic functionalities; that is, the hydrophobic ester bond is formed from hydrophilic hydroxyl and carboxylic functionalities, and the coupling of hydrophilic amine and carboxylic acid functionalities results in a relatively hydrophobic peptide bond. Therefore, in most cross-linked polymer networks, the hydrophilicity and cross-linking density are in a trade-off relation; to increase the hydrophilicity, density of cross-linking must be decreased, which in turn must be accompanied by the sacrifice of mechanical and chemical stability.[40,45] Therefore, the suggested one-step CIP synthetic method in this study can be a simple but powerful tool to generate a robust, hydrophilic surface with excellent mechanical and chemical stability.

The hydrophilic yet mechanically robust CIP film shown here can be applied to surface modification of membranes for oil/water separation. Membranes permeate one component selectively from a mixture while leaving the other component in a retentate phase. For the oil/water separation membrane, therefore, oil or water needs to permeate the membrane selectively.[24,25,46,47] Since the surface energy of water is generally much larger than most of the oil species, it is relatively easy to fabricate a membrane surface to wet oil selectively and repel water in the retentate phase.[48−50] However, since oil is lighter than water in most cases, it is advantageous to make water permeate through the membrane, especially for gravity-driven oil/water separation.[51] To achieve a water-penetrating membrane, it is necessary to make the membrane surface hydrophilic but oil-repellent. In addition, the membrane surface must be robust against the contact with various types of oil species, some of which may solubilize or deform the membrane surface.[24,52,53] Though there are some reports on water-permeating membranes for oil/water separation, a high-performance membrane with excellent separation yield and high permeation flux is still rare.[54−56] The CIP film developed in this study is hydrophilic with excellent solvent resistance to various organic chemicals, which makes it an ideal candidate for an oil/water separation membrane. Furthermore, the conformal coverage characteristics of the iCVD process make the iCVD polymer film suitable for the conformal surface modification of membranes with micro/nanoscale pores.[57] The eco-friendly, cost-efficient iCVD process is also highly beneficial for mass production.[58] Therefore, the iCVD CIP film enables the simple but reliable surface modification of the membrane for oil/water separation.

Among the CIP films, copolymer I with the highest cross-linking density was employed for modifying the oil/water separation membrane surfaces. A 500 nm thick CIP film was deposited on commercially available stainless steel (SUS) mesh with the mesh size of 38 μm via iCVD. SUS mesh is widely adopted for oil/water separation membranes because of its excellent chemical and mechanical robustness as well as uniform pore size.[59] The iCVD process could deposit CIP film on metal mesh, maintaining the highly textured surface of metal mesh, which is not trivial to achieve with liquid-phase methods.[60] Since the applied thickness of the polymer film was only about 1% of the mesh size, the pore size shrinkage due to the applied polymer coating can be minimized. Figure 4a shows the scanning electron microscopy (SEM) images of pristine (left) and p(DMAEMA-*co*-VBC)-coated (right) mesh. The surface morphology of the bare mesh is well maintained even in the membrane coated with iCVD CIP film without any apparent defects or clogging of the pores. Moreover, the cross-sectional SEM image reveals that extremely smooth, conformal polymer film was formed uniformly around the mesh fiber (Figure 4b). The AFM image of p(DMAEMA-*co*-VBC)-coated mesh also confirms the smooth surface of the surface-modified membrane (Figure 4c). The rms roughness was only 0.386 nm even on SUS mesh, fully consistent with the same film on the Si wafer. These results clearly indicate that the surface properties of the membrane can be modified by polymeric coating via iCVD without changing the surface morphology of the SUS membrane.[25]

The surface wetting property of p(DMAEMA-*co*-VBC)-coated mesh was analyzed by monitoring the oil contact angle

DOI: 10.1021/jacs.6b11349
J. Am. Chem. Soc. 2017, 139, 2329−2337

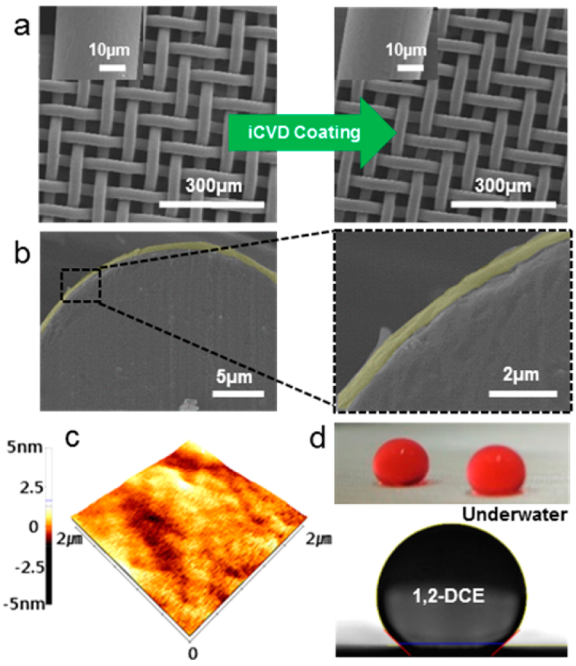

Figure 4. (a) SEM images of stainless steel mesh (38 μm) before (left) and after (right) coating p(DMAEMA-*co*-VBC). Each inset is an enlarged image of the stainless steel mesh. (b) Cross-sectional SEM image of p(DMAEMA-*co*-VBC)-coated single wire in mesh (left). Enlarged view of black square box (right). The fake-colored yellow area indicates the p(DMAEMA-*co*-VBC) thin film having an average thickness of 498 ± 21 nm. (c) AFM image of p(DMAEMA-*co*-VBC) films on mesh. (d) Underwater−oil contact angle on p(DMAEMA-*co*-VBC)-coated mesh. 1,2-Dichloroethane dyed with oil red O was used.

in water. In Figure 4d, the OCA was measured by fully immersing the membrane into water and applying 1,2-dichloroethane drops onto the SUS mesh surface. The average underwater OCA was 136.3 ± 1.4° for 1,2-dichloroethane. Moreover, the oil could be easily removed from the membrane in an underwater environment (see Supplementary Movie 1). The underwater oleophobicity originates from the hydrophilic and hygroscopic nature of the CIP surface. A water layer was trapped at the surface of the CIP-coated membrane by absorbing water in the CIP film. The water layer repels the oil efficiently, while the water permeates through the hydrophilic membrane pores.[23]

The performance of oil/water separation of the p-(DMAEMA-*co*-VBC)-coated SUS membrane was evaluated by using a custom-made apparatus consisting of two glass tubes. The copolymer-coated SUS membrane is placed between the glass tubes with clamp sealing. Oil/water separation was attempted using the aforementioned apparatus, driven solely by gravity without any external pressure (Figure 5a). As expected, the surface-modified membrane could selectively rejects various kinds of oil species from the oil/water mixture such as hexane, hexadecane, and toluene, but water can pass selectively through the membrane pore. The membrane showed practically perfect rejection performance against the oil phase; the calculated separation efficiencies for hexane/water, hexadecane/water, and toluene/water mixtures were as high as 99.6 ± 0.2, 98.8 ± 1.3, and 99.0 ± 0.9%, respectively (Figure 5b). The purity of the filtrate water phase was verified via the Karl Fischer method (ISO 760:2007). The water content of pristine deionized water was 99.98%, which was measured as a control sample. Two filtrates from different batches of hexane/water separation showed 99.94 and 99.96% of water contents, which is virtually identical to that of deionized water (Figure 5c). Analogously, the separation efficiency was measured for 30 cycles using 250 mL of hexane/water mixture (20% v/v) in Figure 5d. For 30 cycles of reuse, the average separation efficiency was 99.5 ± 0.3%, indicating that the membrane can be reused a significant number of times without any apparent degradation of membrane performance. Just 500 nm thick p(DMAEMA-*co*-VBC) film on SUS mesh was sufficient to achieve such an

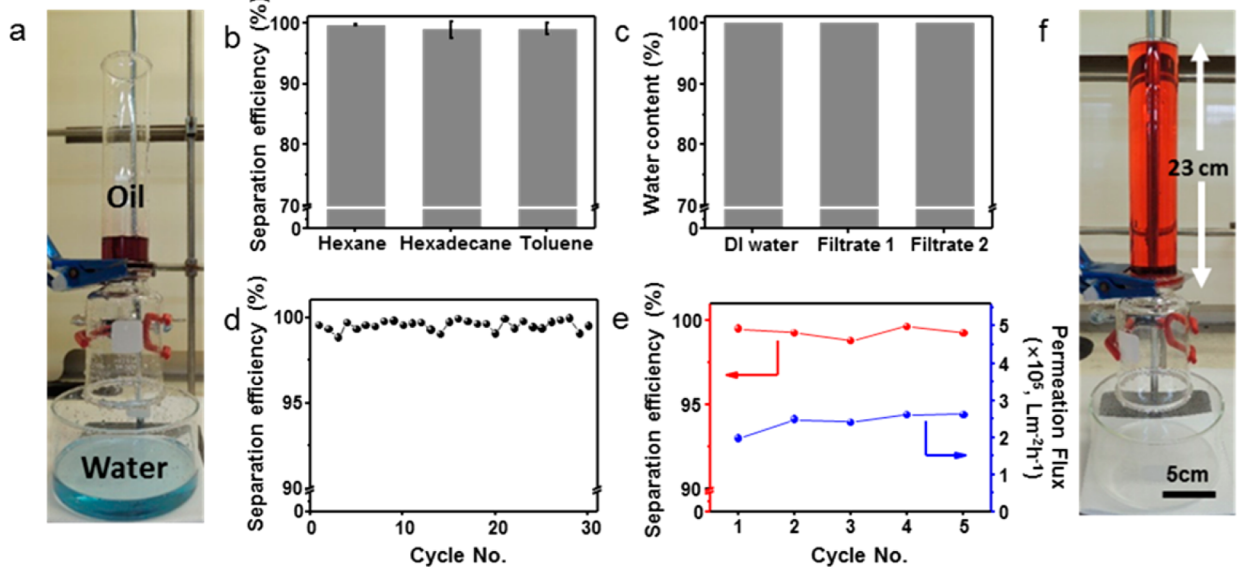

Figure 5. (a) Photograph of oil/water mixture separation using a custom-made apparatus with the p(DMAEMA-*co*-VBC)-coated membrane. (b) Separation efficiency of hexane/water, toluene/water, and hexadecane/water mixture (20% v/v). (c) Water content in filtrate analyzed by the Karl Fischer method (ISO 760:2007). (d) Separation efficiency of hexane/water mixture (20% v/v) for 30 cycles. (e) Separation efficiency (red) and flux (blue) of the p(DMAEMA-*co*-VBC)-coated membrane for five cycles. (f) Digital camera image of the oil resisting property of the p(DMAEMA-*co*-VBC) membrane for hexane, corresponding to the breakthrough pressure of 1.5 kPa.

DOI: 10.1021/jacs.6b11349
J. Am. Chem. Soc. 2017, 139, 2329−2337

Table 2. Summary and Comparison of Recent Reports for Separation Performance

type of membrane	water flux (L m^{-2} h^{-1})	breakthrough pressure (kPa)	separation efficiency (%)	recyclability (cycles)
CIP-coated mesh (this study)	2.32×10^5	1.5 (hexane)	99.5	30
palycorskite-coated mesh[54]	5.40×10^4	1.5 (kerosene)	99.6	50
Ag-coated copper mesh[55]	1.55×10^5	1.8 (hexane)	99.5	NA
zeolite-coated mesh[56]	9.00×10^4	0.73 (cyclohexane)	2−3 ppm	10

excellent performance of oil/water separation. The thin copolymer film retains its original hydrophilicity and underwater oleophobicity even after the 30 reuses of the membrane. In addition, the CIP film-coated mesh did not show any apparent change in surface morphology nor delamination even after the ultrasonication treatment for 40 min. Moreover, the underwater oleophobicity was also well maintained, as shown in Figure S7 in the Supporting Information. This high degree of reusability of the membrane is due to the outstanding chemical and mechanical stability of the ionic cross-linked structures as well as appropriate wetting property of the p(DMAEMA-*co*-VBC) film.

With the separation efficiency, the water permeation flux is another significant factor determining the performance of oil/water separation, especially critical for continuous feed streams. The estimated average water flux was $2.32 \pm 0.09 \times 10^5$ L m^{-2} h^{-1} (see Supplementary Movie 2). Even without any external force, the membrane driven solely by gravity showed a significantly high water permeation flux. The water flux was also maintained with repeated use of the membrane. Five cycles of membrane reuse did not degrade the water permeation flux through the membrane; the membrane maintained average water flux of $2.43 \pm 0.26 \times 10^5$ L m^{-2} h^{-1}, as shown in Figure 5e.

The breakthrough pressure of oil represents the maximum pressure applied to the membrane before the leakage of oils starts through the membrane. In this study, the membrane endured an average 23 cm height of hexane, as shown in Figure 5f, which corresponds to the hexane intrusion pressure of 1.5 kPa, which is quite high for water-permeating oil/water separation membranes. The performance of the oil/water separation membrane developed in this study is summarized in Table 2, compared with the reference data reported previously.

CONCLUSION

In summary, we developed a new synthetic method to generate CIPs in the vapor phase by the iCVD process in a one-step manner. When a nucleophile substitution reaction was introduced during the iCVD process, quaternarization-based cross-linking occurred between tertiary amine and vinylbenzyl chloride-containing vinyl monomers, simultaneously with the free radical polymerization reaction to synthesize the CIP film directly from highly volatile monomers in one step. To the best of our knowledge, this is the first report on the direct synthesis of ionically cross-linked polymers in the vapor phase. The Menshutkin reaction is reportedly unfavorable in the vapor phase due to the lack of polar solvent effects. Therefore, to overcome the activation energy barrier, VBC with highly reactive benzyl chloride was employed in the vapor-phase reaction, resulting in a successful synthesis of CIP. Due to the hydrophilic nature of the ionic cross-linking sites, the copolymer film showed a unique nonlinear hydrophilicity phenomena as well as the hygroscopic property. The hydrophilic cross-linked polymer film showed excellent conformal coverage characteristics onto various nonflat surface morphologies. Moreover, the polymer film showed outstanding chemical stability against various kinds of organic solvents. Finally, the CIP film was applied to fabricate a water-penetrating oil/water separation membrane, which showed an excellent separation efficiency from various kinds of oil/water mixtures, a high degree of reusability up to 30 cycles, and exceptionally high water permeation flux. The superior water permeation flux coupled with the high oil breakthrough pressure of the surface-modified membrane can satisfy the requirements for the continuous operation of membranes, which can play a critical role in reduction of operational cost for large-scaled separation. We believe that the one-step synthesized CIP film in the vapor phase can provide an important idea to generate other new types of CIP films.

ASSOCIATED CONTENT

Supporting Information

The Supporting Information is available free of charge on the ACS Publications website at DOI: 10.1021/jacs.6b11349.

FT-IR, ^{1}H NMR and GPC data of pVBC; XPS data of p(CEA-*co*-DMAEMA) to compare reactivity with p(DMAEMA-*co*-VBC) in the iCVD process (PDF)

Supplementary Movie 1 (AVI)

Supplementary Movie 2 (AVI)

AUTHOR INFORMATION

Corresponding Author

*sgim@kaist.ac.kr

ORCID

Sung Gap Im: 0000-0001-7562-2929

Author Contributions

†M.J. and J.S. contributed equally.

Notes

The authors declare no competing financial interest.

ACKNOWLEDGMENTS

This work was supported by the Advanced Biomass R&D Center of Global Frontier Project funded by the Ministry of Science, ICT and Future Planning (ABC-2010-0029728). This work was also supported by Wearable Platform Materials Technology Center (WMC) funded by the National Research Foundation of Korea (NRF) Grant of the Korean Government (MSIP) (No. 2016R1A5A1009926).

REFERENCES

(1) Yuan, J. Y.; Mecerreyes, D.; Antonietti, M. *Prog. Polym. Sci.* **2013**, *38*, 1009−1036.

(2) Lu, J. M.; Yan, F.; Texter, J. *Prog. Polym. Sci.* **2009**, *34*, 431−448.

(3) Yuan, J. Y.; Antonietti, M. *Polymer* **2011**, *52*, 1469−1482.

(4) Hemp, S. T.; Zhang, M. Q.; Allen, M. H.; Cheng, S. J.; Moore, R. B.; Long, T. E. *Macromol. Chem. Phys.* **2013**, *214*, 2099−2107.

(5) Fan, F.; Wang, Y. Y.; Hong, T.; Heres, M. F.; Saito, T.; Sokolov, A. P. *Macromolecules* **2015**, *48*, 4461−4470.

(6) Green, O.; Grubjesic, S.; Lee, S. W.; Firestone, M. A. *Polym. Rev.* **2009**, *49*, 339−360.
(7) Kolhe, S. M.; Kumar, A. *Radiat. Phys. Chem.* **2007**, *76*, 901−906.
(8) Zhao, J. M.; Duan, H. B.; Jiang, R. J. *Corros. Sci.* **2015**, *91*, 108−119.
(9) Hwang, S. K.; Park, T. J.; Kim, K. L.; Cho, S. M.; Jeong, B. J.; Park, C. *ACS Appl. Mater. Interfaces* **2014**, *6*, 20179−20187.
(10) Li, Y. Q.; Song, Y.; Zhang, X. Y.; Wu, X. X.; Wang, F.; Wang, Z. Y. *Macromol. Chem. Phys.* **2015**, *216*, 113−121.
(11) Zhao, J.; Ma, Y. H.; Hou, X. D.; Li, L. Q.; Zheng, P. F.; Li, C. Y. *J. Solid State Electrochem.* **2015**, *19*, 1571−1578.
(12) Shaplov, A. S.; Marcilla, R.; Mecerreyes, D. *Electrochim. Acta* **2015**, *175*, 18−34.
(13) Lan, C. H.; Fang, J.; Guan, Y. J.; Zhou, H. L.; Zhao, J. B. *J. Power Sources* **2015**, *295*, 259−267.
(14) Merle, G.; Wessling, M.; Nijmeijer, K. *J. Membr. Sci.* **2011**, *377*, 1−35.
(15) Hong, W.; Meis, C.; Heflin, J. R.; Montazami, R. *Sens. Actuators, B* **2014**, *205*, 371−376.
(16) Zhou, F.; Qin, X. S.; Li, Y. C.; Ren, L. X.; Zhao, Y. H.; Yuan, X. Y. *Appl. Surf. Sci.* **2015**, *347*, 231−241.
(17) Zhou, W.; Ma, K. Q.; Tang, L. H.; Li, F.; Huang, L.; Chen, J. H. *J. Appl. Polym. Sci.* **2014**, *131*, 41002.
(18) Nakajima, H.; Ohno, H. *Polymer* **2005**, *46*, 11499−11504.
(19) Bara, J. E.; Hatakeyama, E. S.; Gabriel, C. J.; Zeng, X. H.; Lessmann, S.; Gin, D. L.; Noble, R. D. *J. Membr. Sci.* **2008**, *316*, 186−191.
(20) Chan, K.; Gleason, K. K. *Langmuir* **2005**, *21*, 8930−8939.
(21) Aschenbrenner, O.; Supasitmongkol, S.; Taylor, M.; Styring, P. *Green Chem.* **2009**, *11*, 1217−1221.
(22) Tenhaeff, W. E.; Gleason, K. K. *Adv. Funct. Mater.* **2008**, *18*, 979−992.
(23) Xue, Z. X.; Cao, Y. Z.; Liu, N.; Feng, L.; Jiang, L. *J. Mater. Chem. A* **2014**, *2*, 2445−2460.
(24) Yuan, T.; Meng, J. Q.; Hao, T. Y.; Wang, Z. H.; Zhang, Y. F. *ACS Appl. Mater. Interfaces* **2015**, *7*, 14896−14904.
(25) Kota, A. K.; Kwon, G.; Choi, W.; Mabry, J. M.; Tuteja, A. *Nat. Commun.* **2012**, *3*, 1025.
(26) Xue, Z. X.; Wang, S. T.; Lin, L.; Chen, L.; Liu, M. J.; Feng, L.; Jiang, L. *Adv. Mater.* **2011**, *23*, 4270−4273.
(27) Tao, R.; Anthamatten, M. *Langmuir* **2012**, *28*, 16580−16587.
(28) Mao, Y.; Gleason, K. K. *Langmuir* **2004**, *20*, 2484−2488.
(29) Oh, Y. J.; Jeong, C. J.; Sharker, S. M.; Lee, S. Y.; In, I.; Park, S. Y. *Surf. Interface Anal.* **2015**, *47*, 259−264.
(30) Meng, J. Q.; Zhang, X.; Ni, L.; Tang, Z.; Zhang, Y. F.; Zhang, Y. J.; Zhang, W. *Desalination* **2015**, *359*, 156−166.
(31) Suzer, S.; Birer, O.; Sevil, U. A.; Guven, O. *Turk. J. Chem.* **1998**, *22*, 59−65.
(32) Castejon, H.; Wiberg, K. B. *J. Am. Chem. Soc.* **1999**, *121*, 2139−2146.
(33) Giri, S.; Inostroza-Rivera, R.; Herrera, B.; Nunez, A. S.; Lund, F.; Toro-Labbe, A. *J. Mol. Model.* **2014**, *20*, 2353.
(34) Su, P. F.; Ying, F. M.; Wu, W.; Hiberty, P. C.; Shaik, S. *ChemPhysChem* **2007**, *8*, 2603−2614.
(35) Jiang, L. Z.; Orimoto, Y.; Aoki, Y. *J. Chem. Theory Comput.* **2013**, *9*, 4035−4045.
(36) Sykes, P. *Guidebook to Mechanism in Organic Chemistry*, 6th ed.; Wiley: New York, 1986; pp 82−87.
(37) Erden, I.; Gronert, S.; Keeffe, J. R.; Ma, J. X.; Ocal, N.; Gartner, C.; Soukup, L. L. *J. Org. Chem.* **2014**, *79*, 6410−6418.
(38) Yang, R.; Xu, J. J.; Ozaydin-Ince, G.; Wong, S. Y.; Gleason, K. K. *Chem. Mater.* **2011**, *23*, 1263−1272.
(39) Li, Y.; Herring, A. M.; Knauss, D. M. *ECS Trans.* **2014**, *59*, 307−313.
(40) Kwak, M. J.; Oh, M. S.; Yoo, Y.; You, J. B.; Kim, J.; Yu, S. J.; Im, S. G. *Chem. Mater.* **2015**, *27*, 3441−3449.
(41) Moon, H.; Seong, H.; Shin, W. C.; Park, W. T.; Kim, M.; Lee, S.; Bong, J. H.; Noh, Y. Y.; Cho, B. J.; Yoo, S.; Im, S. G. *Nat. Mater.* **2015**, *14*, 628−635.
(42) Melo, A.; Alfaia, A. J. I.; Reis, J. C. R.; Calado, A. R. T. *J. Phys. Chem. B* **2006**, *110*, 1877−1888.
(43) Vengatesan, S.; Santhi, S.; Sozhan, G.; Ravichandran, S.; Davidson, D. J.; Vasudevan, S. *RSC Adv.* **2015**, *5*, 27365−27371.
(44) Cao, Y. C.; Wang, X.; Mamlouk, M.; Scott, K. *J. Mater. Chem.* **2011**, *21*, 12910−12916.
(45) Sun, M.; Wu, Q. Y.; Xu, J.; He, F.; Brown, A. P.; Ye, Y. M. *J. Mater. Chem. B* **2016**, *4*, 2669−2678.
(46) Wang, Z. X.; Lau, C. H.; Zhang, N. Q.; Bai, Y. P.; Shao, L. *J. Mater. Chem. A* **2015**, *3*, 2650−2657.
(47) Gao, S. J.; Shi, Z.; Zhang, W. B.; Zhang, F.; Jin, J. *ACS Nano* **2014**, *8*, 6344−6352.
(48) Zhang, J. P.; Seeger, S. *Adv. Funct. Mater.* **2011**, *21*, 4699−4704.
(49) Kwon, G.; Post, E.; Tuteja, A. *MRS Commun.* **2015**, *5*, 475−494.
(50) You, J. B.; Yoo, Y.; Oh, M. S.; Im, S. G. *ACS Appl. Mater. Interfaces* **2014**, *6*, 4005−4010.
(51) Kwon, G.; Kota, A. K.; Li, Y. X.; Sohani, A.; Mabry, J. M.; Tuteja, A. *Adv. Mater.* **2012**, *24*, 3666−3671.
(52) Zhang, F.; Zhang, W. B.; Shi, Z.; Wang, D.; Jin, J.; Jiang, L. *Adv. Mater.* **2013**, *25*, 4192−4198.
(53) Yang, R.; Moni, P.; Gleason, K. K. *Adv. Mater. Interfaces* **2015**, *2*, 1400489.
(54) Li, J.; Yan, L.; Li, H. Y.; Li, W. J.; Zha, F.; Lei, Z. Q. *J. Mater. Chem. A* **2015**, *3*, 14696−14702.
(55) Liu, L. Y.; Chen, C.; Yang, S. Y.; Xie, H.; Gong, M. G.; Xu, X. L. *Phys. Chem. Chem. Phys.* **2016**, *18*, 1317−1325.
(56) Wen, Q.; Di, J. C.; Jiang, L.; Yu, J. H.; Xu, R. R. *Chem. Sci.* **2013**, *4*, 591−595.
(57) Kwak, M. J.; Yoo, Y.; Lee, H. S.; Kim, J.; Yang, J. W.; Han, J. I.; Im, S. G.; Kwon, J. H. *ACS Appl. Mater. Interfaces* **2016**, *8*, 600−608.
(58) Schropp, R. E. I. *Thin Solid Films* **2015**, *595*, 272−283.
(59) Gao, C. R.; Sun, Z. X.; Li, K.; Chen, Y. N.; Cao, Y. Z.; Zhang, S. Y.; Feng, L. *Energy Environ. Sci.* **2013**, *6*, 1147−1151.
(60) Volodin, P.; Kondyurin, A. *J. Phys. D: Appl. Phys.* **2008**, *41*, 065306.

DOI: 10.1021/jacs.6b11349
J. Am. Chem. Soc. 2017, 139, 2329−2337